Materials Today 87 (2025) 66–76

Contents lists available at ScienceDirect

Materials Today

journal homepage: www.elsevier.com/locate/mattod

Research

Programmable magnetic hydrogel robots with drug delivery and physiological sensing capabilities

Hegeng Li [a,b], Shaojun Jiang [b], Qiyu Deng [b], Wei Li [b], Weixin Zhang [b,d], Hengjia Zhu [b], Zhipeng Zhao [b], Yiyuan Zhang [c], Liqiu Wang [c,*], Lizhi Xu [b,d,e,**]

[a] School of Mechanical and Electronic Engineering, Wuhan University of Technology, Wuhan, China
[b] Department of Mechanical Engineering, The University of Hong Kong, Hong Kong Special Administrative Region of China
[c] Department of Mechanical Engineering, The Hong Kong Polytechnic University, Hong Kong Special Administrative Region of China
[d] Advanced Biomedical Instrumentation Centre Limited, Hong Kong Special Administrative Region of China
[e] Materials Innovation Institute for Life Sciences and Energy (MILES), The University of Hong Kong Shenzhen Institute of Research and Innovation (HKU-SIRI), Shenzhen 518057, P.R. China

ARTICLE INFO

Keywords:
Magnetic robots
Magnetic hydrogels
Implantable platforms
Drug delivery
Multifunctional sensing

ABSTRACT

Magnetic hydrogels are promising materials for the construction of magnetic soft robots applied in robotic systems and implantable devices. However, programming geometric shapes and magnetization profiles of magnetic hydrogel robots (MHRs), as well as integrating functional modules into robotic systems, remain challenging. Here, we report an assembly strategy for MHRs with programmable magnetization profiles and geometries, constructed from discrete integration of magnetized hydrogels and a patterned elastomer membrane based on covalent crosslinking. The resulting robots exhibit sophisticated deformations under varying magnetic fields, enabling effective carrying and delivery of solid drugs. Moreover, the proposed fabrication method preserves the highly porous and hydrophilic microstructures of the hydrogels, facilitating loading, adhesion, and transport of liquid drugs in combination with magnetic properties. Besides, integrating ultrathin and multifunctional microfabricated electronics into the MHRs is also achieved for physiological sensing and simulation, which has negligible effects on their intrinsic mechanics and deformability. The introduction of these magnetic materials and fabrication methods can shed new insights for the development of advanced biomedical tools and robotic systems.

Magnetic soft robots capable of navigating in complex and constrained spaces have emerged as promising biomedical tools due to their mechanical compliance, fast response, and wireless control [1–5]. Magnetic composite materials composed of hard-magnetic particles [i.e., neodymium-iron-boron (NdFeB)] and soft matrixes have been employed in the construction of magnetic soft robots with designed geometric shapes and magnetization distributions [6,7]. In current practices, elastomers are generally selected as soft matrixes due to their excellent processability and material compatibility [8,9]. However, elastomers can only provide mechanical support and are limited in their contributions to the biomedical applications of magnetic soft robots. In contrast, hydrogels, as an alternative candidate material, exhibit greater potential due to their high water content, tissue-like mechanical properties and excellent biocompatibility, which make them particularly advantageous for drug delivery and implantable devices [10–14]. Nevertheless, further efforts are required to overcome the challenges associated with fabricating magnetic hydrogel robots (MHRs) with heterogeneous structures and programmable magnetization profiles.

Indeed, extensive methods have been developed over the past decade to fabricate magnetic soft robots with specific geometries and magnetization profiles. For example, the magnetic material with planar structures is first deformed into a desired temporary shape using a template, followed by the application of a strong magnetic field to magnetize the material in the deformed state [15–17]. Nevertheless, this template-assisted strategy is prone to form continuous magnetization profiles for simple planar structures, resulting in some gaps between the desired shapes and the actual shapes under magnetic actuation, partly due to the inability of the external magnetic field to exceed the

* Corresponding author.
** Corresponding author at: Department of Mechanical Engineering, The University of Hong Kong, Hong Kong Special Administrative Region of China.
E-mail addresses: liqiu.wang@polyu.edu.hk (L. Wang), xulizhi@hku.hk (L. Xu).

https://doi.org/10.1016/j.mattod.2025.05.008
Received 11 November 2024; Received in revised form 31 December 2024; Accepted 1 May 2025
Available online 16 May 2025

coercivity of the material at certain angles. Extrusion-based 3D printing offers another approach for controlling magnetization patterns by applying a weak magnetic field during the printing process, but the printing technique has specific requirements concerning the rheological properties of the inks and post-treatment procedures, which may limit their compatibility with magnetic hydrogels [18–20]. Alternatively, tiny building blocks of magnetic elastomers, fabricated by various fabrication techniques, can be discretely adhered to other materials to construct magnetic robots with designed magnetization distributions [21,22]. However, such an adhesion mechanism is not applicable to hydrogels that contain significant amounts of water.

Besides, previous research primarily focused on designing geometric shapes and magnetization profiles of magnetic soft robots, with insufficient attention given to integrating sensing functions [23–27]. Considering the high requirements for movement ability while maintaining lightweight structures, the introduction of the sensing modules cannot be at the expense of the flexible deformability of the robots. Moreover, the sensing unit should be closely integrated with the robot to prevent delamination during the deformation process. The physiological sensing capabilities provided by multifunctional microsensors can be combined with the drug delivery derived from magnetic hydrogels to complete a closed-loop system encompassing sensing, treatment, and actuation.

Herein, we report a general method for the construction of MHRs with programmable geometries and magnetization distributions. The magnetized hydrogels are discretely integrated onto a patterned elastomer membrane by establishing robust interfaces between the magnetic hydrogels and the elastomers through covalent crosslinking. The resultant programmable MHRs can realize reversible transformations between complex 3D shapes, and the flexible deformations of structures are capable of carrying solid drugs and then transporting them on demand. Moreover, the reported fabrication method also retains highly porous and hydrophilic networks of the hydrogels, allowing the loading and distribution of liquid medications. In addition, highly integrated and miniaturized microfabricated electronics can be seamlessly integrated into the MHRs to enable physiological sensing and stimulation

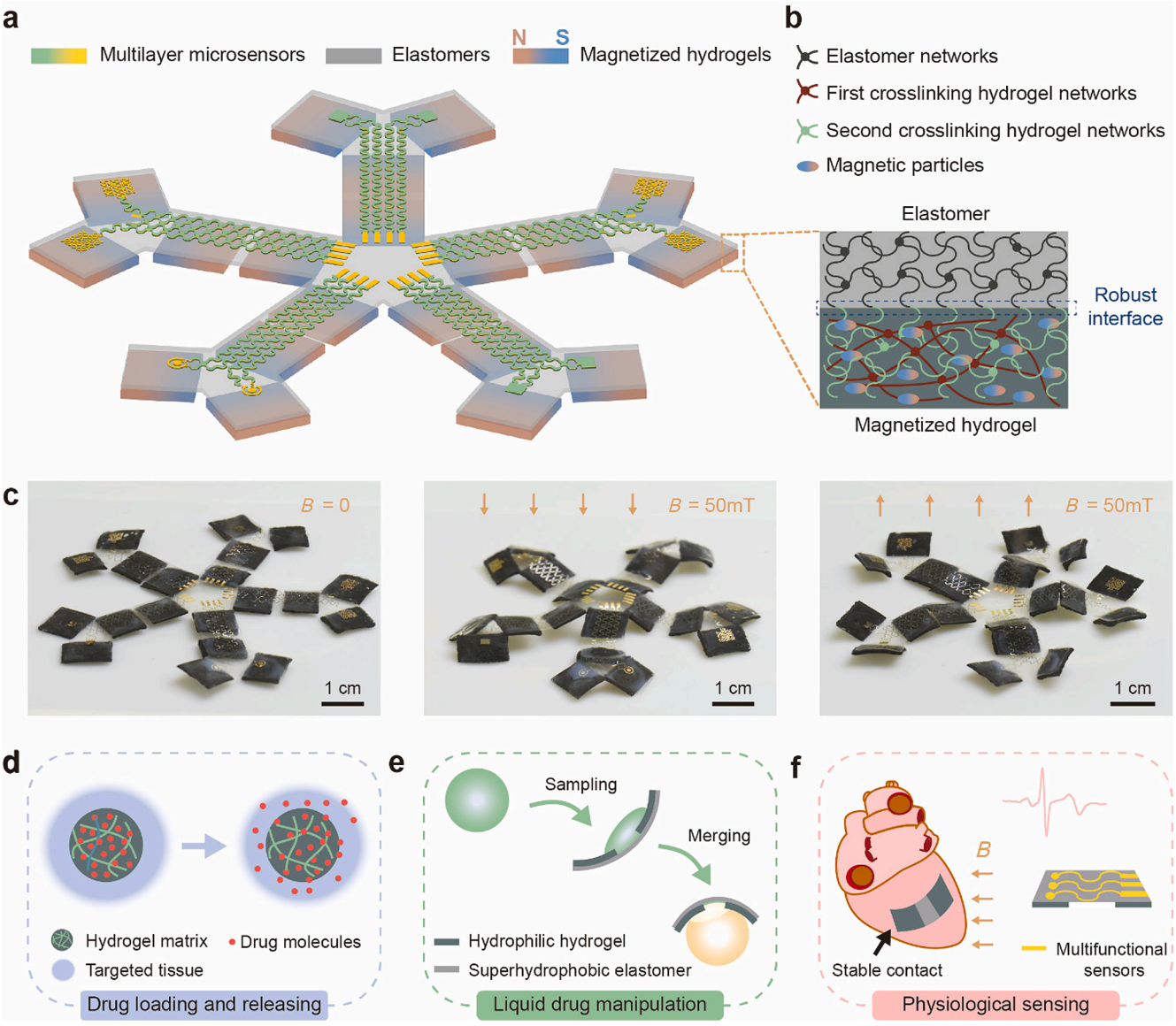

Fig. 1. Schematic and applications of programmable magnetic hydrogel robots (MHRs). (a) Schematic illustration of an example five-legged MHR consisting of magnetized hydrogels, elastomers, and multilayer microsensors. (b) Schematic illustration of the robust interface between magnetized hydrogels and elastomers. (c) Different mechanical deformation of the five-legged MHR under varying applied magnetic fields. The MHRs can be designed for drug loading and releasing (d), liquid drug manipulation (e), and physiological sensing (f).

without compromising the deformability and motility of the MHRs. The development of magnetic materials and fabrication methods provides a wide range of opportunities for the construction of implantable electronic platforms and robotic manipulations.

Results

A representative five-legged robot, composed of 20 rectangular pieces of magnetized hydrogels and a patterned elastomer film, was developed to describe the proposed fabrication approach (Fig. 1a). The hydrogel precursor solutions and hard-magnetic particles were mixed by a stepwise assembly and then cast in a designed mold or coated as a film. Pre-shaped magnetic hydrogels can be created following the formation of the first crosslinking network, subsequently magnetized using an impulse magnetizer. The resulting pre-shaped magnetized hydrogels with high porosity allow for the infiltration of other hydrogel monomers to construct second crosslinking networks with other materials. This means that the magnetized hydrogels can serve as the building blocks for robots with desired geometries and magnetization distributions. On the other hand, the elastomer surfaces (e.g., those from polydimethylsiloxane or PDMS) should be treated with benzophenone to prevent oxygen inhibition, which could impede the covalent crosslinking with hydrogel networks. Under UV irradiation, benzophenone acts as a grafting agent that can covalently crosslink with the second hydrogel networks on the elastomer surfaces. Here, the treated elastomer can bind each hydrogel segment together like adhesive tape at designated positions and magnetization distribution to form a cohesive robot (Fig. S1). To guarantee accuracy in the geometry of the robots, 3D-printed molds were utilized to assist in the assembly process (Fig. S2). Moreover, this assembly method is also suitable for millimeter-scale miniature robots. With precise manipulation, we can assemble MHRs that are on the same order of magnitude in size as human hair (Fig. S3). The detailed synthesis procedures of the magnetized hydrogel and assembly approach of the robots can be found in the 'Methods' section.

The robust interfaces between magnetized hydrogels and elastomers are formed via covalent crosslinking, preventing mechanical failure of the robots during reversible deformation (Fig. 1b). The elastomer provides the overall mechanical support for the robots, while the discretely distributed magnetized hydrogels generate the driving force from external magnetic fields. As a result, the five-legged robot can carry out deformations such as folding and unfolding in response to the variation of the externally applied magnetic fields (Fig. 1c). The capability of the reversible transformation between complex 3D shapes allows the robot to perform crawling motion on the land, indicating that the shape-morphing structures endow the locomotion abilities of the MHRs (Fig. S4 and Movie S1). Furthermore, the proposed fabrication method still retains the highly hydrophilic and porous microstructures of the magnetic hydrogels, enabling a set of previously inaccessible applications. For instance, the magnetic hydrogels with high porosity act as a natural carrier for soluble drugs, and the MHRs can release drugs when and where needed (Fig. 1d). The highly hydrophilic hydrogel networks exhibit strong adhesion to liquid droplets, which facilitates the construction of a versatile manipulation platform for liquid drugs and biological reactions (Fig. 1e). Besides, the highly integrated and ultrathin microelectronics, fabricated on the silicon wafers, can be transfer-printed onto the elastomer, followed by integration with magnetized hydrogel for the construction of MHRs. The integrated microsensors not only have negligible effects on the mechanical deformation of the robot but also can establish a stable contact with the targeted tissue under a magnetic field to realize physiological sensing and stimulation (Fig. 1c and f).

Compared with soft-magnetic materials, hard-magnetic materials possess the ability to retain high remnant magnetization and coercivity, leading to a stable and permanent magnetic source. The high coercivity grants them great resistance to being demagnetized even when exposed to external magnetic fields, which means that the hard-magnetic materials are ideal choices for building magnetic soft robots. However, the high coercivity mainly stems from the high iron contents, which are susceptible to being corroded in water-rich hydrogels. Therefore, a thin shell of silica was prepared through the condensation reaction of tetraethyl orthosilicate (TEOS) to wrap around the NdFeB particle to prevent oxidation. The transmission electron microscope (TEM) testing and energy dispersive spectrometry (EDS) mapping were employed to characterize the silica shell about ~10 nm. The leaching experiment also identified the effectiveness of the silica coating layer, as there were no visible changes observed in the coated particles after soaking for 60 days (Fig. S5). Besides, a leaching experiment was conducted to evaluate the risk of magnetic particle leakage. Magnetic hydrogels were immersed in fresh cell culture medium for 48 h to absorb any released chemical compounds. The culture medium containing the released compounds was then used for NIH 3T3 fibroblasts culture. The results showed excellent cell proliferation and viability on days 1, 3, and 5, confirming the non-toxicity of the leaching solution (Fig. S6).

The robustness of the interfaces between the magnetized hydrogels and elastomers directly affects how well and durable the MHRs are. To quantify the adhesion energy of the interface between magnetized hydrogel and elastomer, the 180° peeling test was conducted to measure their interfacial toughness (Fig. S7). The measured values of interfacial fracture energy consistently exceeded 120 J/m^2 across varying magnetic particle contents, indicating sufficient adhesion between magnetized hydrogels and elastomers (Fig. 2a). Referring to the structure of the five-legged MHRs, magnetized hydrogels can be regarded as the legs of the robots, providing mechanical support and serving as a power source for deformations and locomotion. Therefore, we proceeded to characterize the magnetic and mechanical properties of the magnetic hydrogels. A vibrating sample magnetometer (VSM) was used to characterize the magnetic properties of the hydrogels in Fig. S8, revealing hard-magnetic properties with high remanent magnetic moments and coercivity. With an increase in magnetic particle weight fraction from 10 % to 40 %, the resulting remanent magnetization linearly fluctuates from 13 kA m^{-1} to 65 kA m^{-1}, which can supply sufficient power for the deformation of MHRs (Fig. 2b). The mechanical properties of the pre-shaped magnetized hydrogels are shown in Fig. 2c and Fig. S9. The pre-shaped hydrogels exhibit high stiffness, ranging from 81 kPa to 156 kPa, depending on the solid content of magnetic particles. Additionally, the mechanical properties of the hydrogel are further enhanced after the second cross-linking. Therefore, the high elastic modulus of the magnetized hydrogels can offer enough mechanical support during robot folding or movement. Furthermore, other robust magnetic hydrogels, such as magnetic cellulose hydrogels, can also be coupled with elastomers to construct MHRs, given the versatility of the preparation method. The interfacial toughness between cellulose hydrogels and elastomers, along with the mechanical properties of magnetic cellulose hydrogels, make them well-suited for constructing MHRs (Fig. S10).

A simplified model was developed to describe the deformation behaviors of the MHRs. Two magnetized hydrogels are discretely distributed on both sides of a rectangular elastomer sheet to form a simply supported beam model (Fig. 2d and Fig. S11a). The magnetized hydrogels can be regarded as the legs of the robots, while the elastomer sheet, without bonding with hydrogels, functions as a hinge in the model. In an external uniform magnetic field, the leg section rotates like a pair of dipoles, which would drive the hinge to bend by overcoming its inherent stiffness resistance, as illustrated in Fig. 2e. Therefore, the bending moment can be expressed as $\boldsymbol{\tau} = \boldsymbol{\mu} \times \mathbf{B}$, where $\mathbf{B}$ denotes the magnetic flux density of the applied magnetic field, and $\boldsymbol{\mu}$ denotes the magnetic dipole moment. The bending deflection y of the hinge describes the degree of deformation of the robots (Fig. S11b) and the deflection is highly dependent on the thickness of the elastomer according to our computational model. The imposed bending moment cannot cause the elastomer to bend when the thickness exceeds the critical value. In cases when the thickness is suitable or thin,

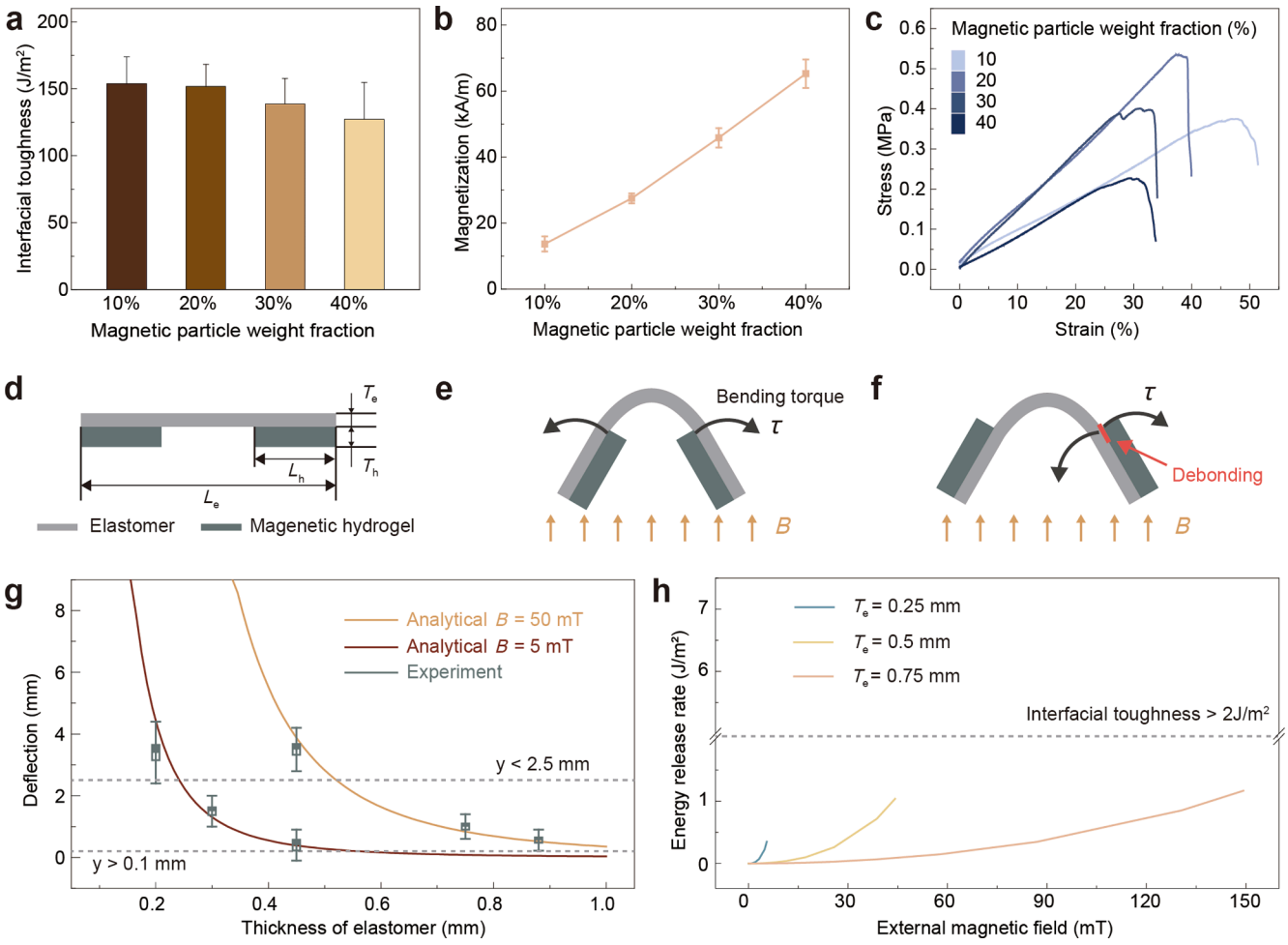

Fig. 2. Magnetic and mechanical characterizations of MHRs. (a) Measured the interfacial toughness between magnetized hydrogels and elastomers, with the magnetic particle weight fraction varying from 10% to 40%. (b) Effect of the weight fraction on the magnetization of the magnetic hydrogels. (c) Tensile response of the magnetized hydrogels with various weight fractions. (d) Side view of the theoretical model for the MHRs. L_e, length of elastomer; L_h, length of magnetized hydrogel; T_e, thickness of elastomer; T_h, thickness of magnetized hydrogel. (e) Frontal bending deformation is driven by the applied magnetic fields. Bending moment τ is the result of magnetic hydrogels responding to magnetic fields. (f) Reversed bending deformation is driven by an opposite magnetic field. There is an energy release rate to drive the separation of hydrogels and elastomers. (g) Analytical and experimental results reveal the relationship between the deflection and thickness of the elastomer beam. (h) The energy release rate is calculated by finite element analysis (FEA) as a function of applied magnetic fields for various thickness elastomers.

deformation can be achieved with a very modest external magnetic field. These theoretical analyses align well with the experimental results (Fig. 2g and Fig. S12), and the analytical model is based on an assumption that the presence of magnetized hydrogels has no influence on the external magnetic field.

On the other hand, the model may undergo reverse deformation, as illustrated in Fig. 2f, during the different locomotion scenarios. The induced bending moments of magnetized hydrogels point away from the interface of the hydrogel and elastomer. Consequently, a crack could potentially occur near the interface edge, and the evaluation of crack extension involves the use of energy release rates. If the energy release rate exceeds the interfacial toughness within the interfacial system, crack propagation occurs, leading to detachment of the magnetized hydrogels from the elastomers. On the contrary, if the energy release rate is lower than the interfacial toughness, the system remains stable. We use finite element analysis (FEA) to calculate the energy release rate of serval models with different elastomer thicknesses (Fig. 2h and Fig. S11c). The resulting values, all below 2 J/m^2, are significantly lower than the measured interfacial toughness (Fig. 2a), indicating that the integration between the magnetized hydrogels and elastomers remains intact under various motions.

The powerful programmability of the proposed fabrication method offers the MHRs with exceptional deformability and multimode locomotion, suggesting their potential for application in robotic manipulation and drug administration. A ribbon-like robot was fabricated with the specific geometrical shape and magnetization profiles. When a uniform magnetic field is applied downward or upward, the ribbon-like structure can transform into an 'm' shape or 'w' shape, respectively (Fig. 3a). The robot can adapt to a variety of working environments by rolling or crawling through different external magnetic fields because of their flexible and reversible deformations (Fig. 3b and Movie S2). Combined with the numerous deformations and movement modes, the robots are capable of performing efficient solid drug distribution operations. When an external magnetic field is applied, the MHR encompasses the capsule-like drug due to structural distortion and then transports it to the intended location (Fig. 3c).

Compared with other magnetic soft robots, the MHRs are capable of loading a large amount of soluble medication due to their highly porous microstructure (Figs. S13 and S14). The magnetized hydrogels were immersed in a high-concentration medicine solution to load soluble drugs within their porous network, allowing controllable release driven by concentration gradients (Fig. 3d). Even drugs with limited water solubility are compatible with our MHR drug-loading system, as the highly hydrophilic and porous microstructure can store both water and

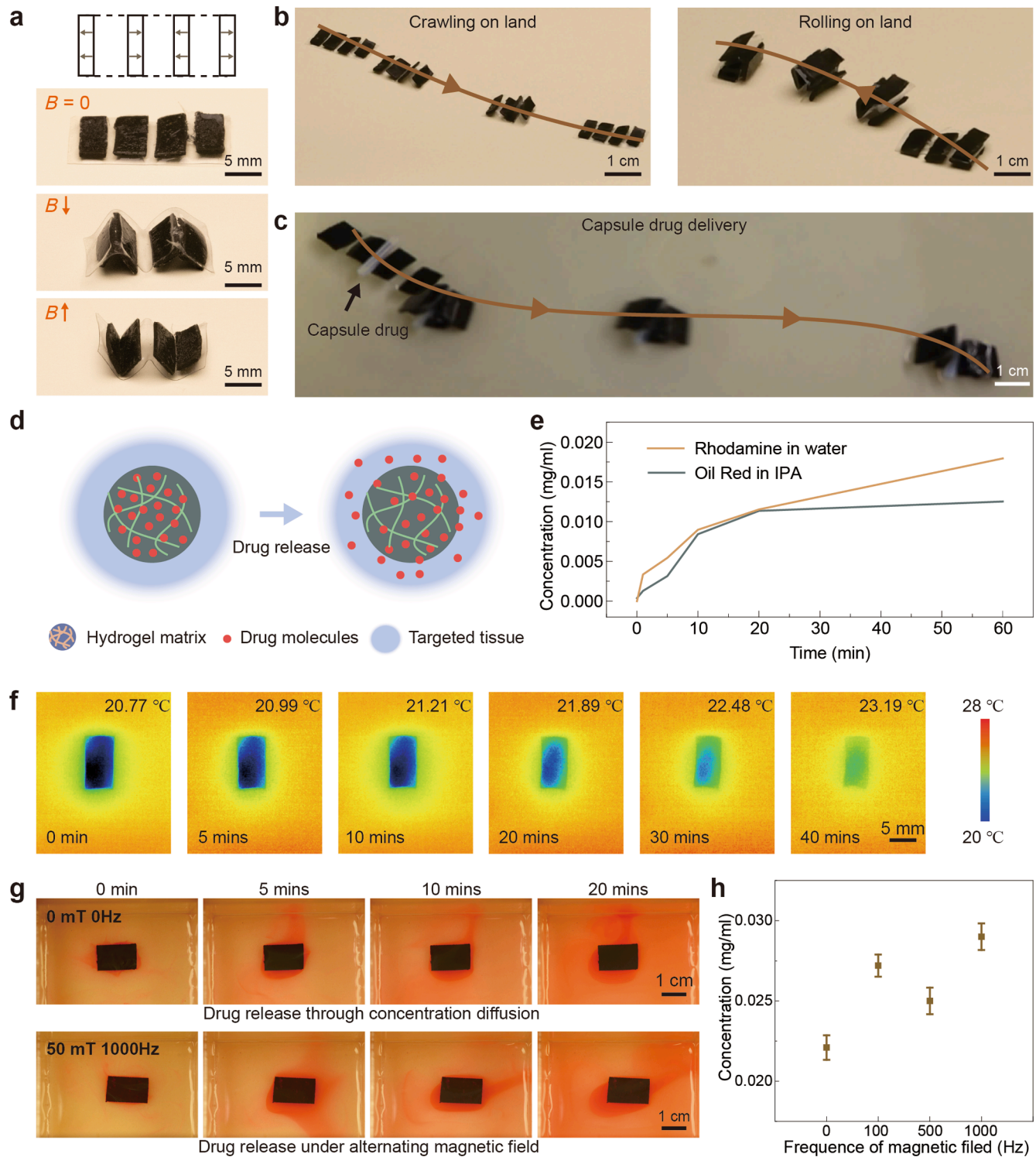

Fig. 3. Drug loading and releasing demonstrations of programmable MHRs. (a) Schematic and experimental results for a ribbon-like robot with 2D geometries showing different magnetic responses at varying magnetic fields. (b) The ribbon-like MHR demonstrates the crawling and rolling locomotion driven by the rotating and moving permanent magnet. (c) The ribbon-like MHR wraps around a capsule-like drug and delivers it to the expected position. (d) Schematic illustration of the soluble drug releasing controlled by concentration diffusion. (e) The release behavior of rhodamine and oil red in water and isopropanol, respectively. (f) Temperature variation of the magnetized hydrogel under an alternating magnetic field at 1000 Hz. (g) Sequential optical images capturing the entire process of soluble drug delivery, including concentration-driven diffusion (top) and diffusion assisted by a 50 mT, 1000 Hz magnetic field (bottom). (h) The relationship between drug release from drug-loaded magnetic hydrogels over 20 min and the frequency of the magnetic field.

organic solvents, significantly expanding the range of drugs that MHRs can accommodate. We used rhodamine and Oil Red as model drugs, dissolved in water and isopropyl alcohol (IPA), respectively. Both drugs demonstrated excellent release performance (Fig. 3e and Fig. S15). Moreover, an alternating magnetic field can heat the hydrogel to control drug release (Fig. 3f), and its excellent tissue transparency makes it highly suitable for such implantable robots. The magnetic hydrogel exhibits different magnetic responses depending on the frequency of the

alternating magnetic field. When the frequency is below 100 Hz, the magnetic hydrogel moves continuously in response to changes in the magnetic field direction, as shown in Movie S3. However, at frequencies above 100 Hz, the hydrogel can no longer respond to the field direction changes and remains stationary. During this stationary phase, the temperature of hydrogel gradually increases over time. Fig. 3g and Fig. S15 show that under an alternating magnetic field, the drug release rate is significantly higher than natural release. Quantitative analysis in Fig. 3h further confirms this observation. Interestingly, the release rate at 100 Hz is faster than at 500 Hz, likely due to slight vibrations of the hydrogel at 100 Hz that further accelerate drug release. In contrast, the hydrogel remains completely stationary at 500 Hz. Under a constant magnetic field strength, higher frequencies result in faster drug release rates from the magnetic hydrogel.

Moreover, the highly hydrophilic networks of the magnetic hydrogels demonstrate strong adhesion for a broad spectrum of liquids (Fig. S17a). Conversely, the elastomers treated with a superhydrophobic solution exhibit poor adhesion to these liquids due to their rough surface topography (Fig. 4b–c and Fig. S17b). As a result, our MHRs are processed into a Janus structure, giving new possibilities for the manipulation of liquid drugs. For instance, two hydrophilic magnetized hydrogels were bonded on both sides of a superhydrophobic elastomer film to construct the Janus MHR, as shown in Fig. 4a. The strong liquid adhesion of the hydrophilic hydrogel networks allows sampling droplets as well as containing droplets in tiny elastomer intermediate containers for transportation. Superhydrophobic glass and elastomer surfaces ensure no residue is left behind during droplet manipulation. Leveraging the Janus property, the robot can float on the surfaces of the droplets to execute the stirring function for efficient mixing. By integrating these functions, the Janus MHR can realize continuous liquid manipulations, as shown in Fig. 4d and Movie S4.

The versatility of the reported fabrication method also enables the

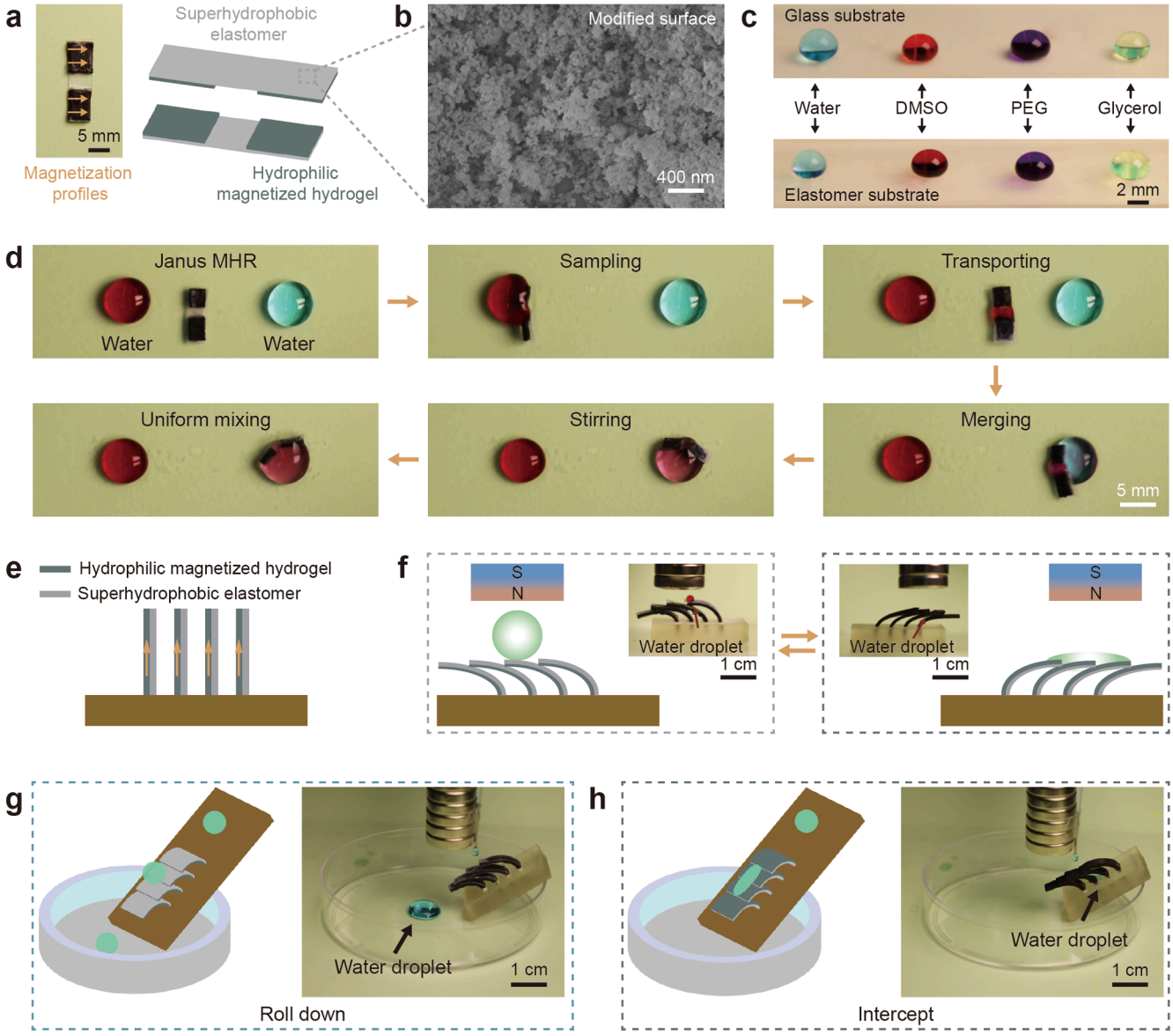

Fig. 4. Janus MHRs performing liquid drug manipulation. (a) Images of a Janus MHR; orange arrows represent its magnetization profiles, the grey side is a superhydrophobic elastomer and the deep green sides are hydrophilic magnetized hydrogels. (b) Scanning electron microscope (SEM) image of superhydrophobic coating on the elastomer surface. (c) Images of droplets of water, DMSO, PEG and glycerol on the glass and elastomer both modified by superhydrophobic coating. (d) The versatile droplet manipulation integration of the Janus robot, including sampling, transport, merging, and stirring. (e) Schematic of a magnetically responsive water droplet switch with 3D geometries. (f) Schematics of switchable wettability of the 3D MHR. Water droplets can roll down or be intercepted when touching the superhydrophobic elastomer (g) or hydrogel (h).

creation of MHRs with 3D structures, facilitating a wider range of liquid manipulation possibilities. Here, a unique magnetically sensitive water droplet switch was created, as depicted in Fig. 4e. In this setup, four pieces of magnetized hydrogel-elastomer hybrid are vertically inserted into a 3D printing mold. By modulating the distribution of the magnetic fields, these hybrids can flex in different directions, yielding a continuous surface that alternates between superhydrophobic and hydrophilic states (Fig. 4f and Movie S5). When oriented with the superhydrophobic surfaces upwards under the influence of external magnetic fields, water droplets can effortlessly roll down due to the teeny adhesion (Fig. 4g). On the contrary, when the magnetized hydrogel sides face upwards, the water switch demonstrates remarkable interception capabilities owing to the hydrophilic properties of the magnetized hydrogels (Fig. 4h). Such dynamically adaptable surfaces hold significant promise for applications in fog collection and droplet manipulation.

Besides, the electronic sensors constitute an essential component of soft robots, which can realize electrophysiological sensing and simulation, as well as provide feedback for drug delivery. The magnetic soft

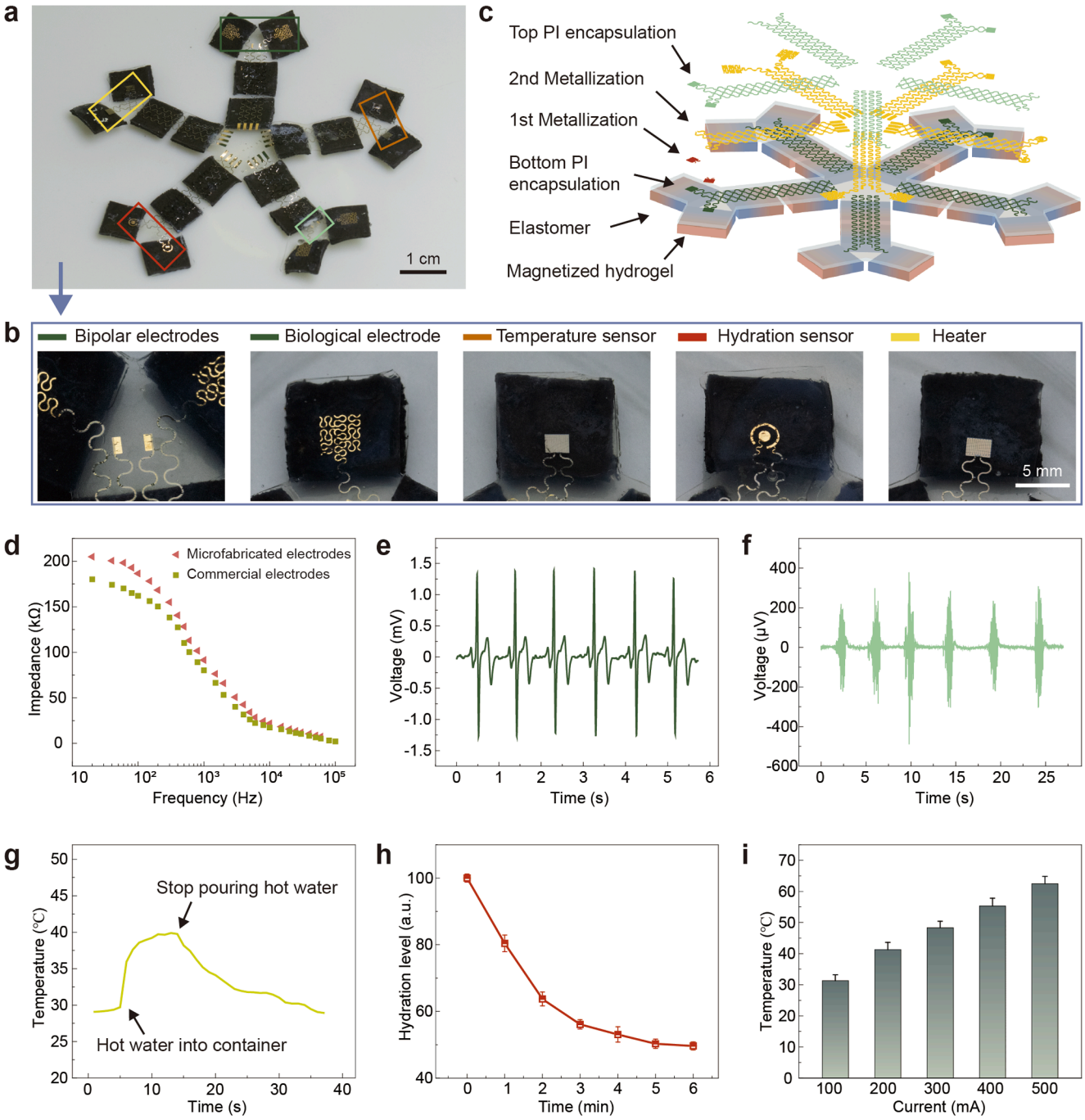

Fig. 5. Multifunctional microsensors integrated onto the MHRs. (a) An optical image showing the multifunctional electronics integrated onto a five-legged robot. (b) Enlarged images of the multifunctional electronics in (a) including bipolar electrodes, biological electrode, temperature sensor, hydration sensor, and heater. (c) Exploded schematic of the multifunctional electronics fabricated layer by layer. (d) Skin impedances measured with commercial electrodes and microfabricated electrodes. ECG signals (e) and EMG signals (f) recorded by biological electrodes on the MHRs. (g) Water temperature variation measured with a temperature sensor on the MHRs. (h) Decay of skin hydration after applying moisturizing lotion on the volunteer's arm, characterized by a hydration sensor on the MHRs. (i) Temperature variation of the heater at a current varying from 100 to 500 mA.

robot is a potential implantable platform because the implantable device can form a close and controllable contact with tissue in wet environment of human body. The continuous elastomer membranes serve as an ideal platform for integrating multifunctional microfabricated sensors into the MHRs. Specifically, microfabricated electronics were made layer by layer on a silicon wafer via photolithography and etching techniques, before being transfer-printed onto the elastomers (Fig. 5c and Fig. S18). Each layer bestows distinct functionalities upon the multifunctional electronics. For instance, the 1st metallization layer is tailored for the temperature sensors and the 2nd metallization layer caters to other sensing functions (Figs. S19 and S20). Moreover, the polyimide (PI) layer can selectively encapsulate the electroactive layers to prevent the collection of invalid signals and facilitate the chemical grafting of the surface. As a proof of concept, an electronic array was devised for the five-legged structural robot, comprising two pairs of bipolar electrodes, four biological electrodes, two temperature sensors, two hydration sensors, and two heaters (Fig. 5a and b). These sensors are meticulously arranged on the five legs of the robot, respectively. The contact impedance between the microfabricated electrodes and the skin is about 200 kΩ at 100 Hz, similar to the commercial gel electrodes (Fig. 5d). Consequently, the high-quality electrocardiogram (ECG) and electromyogram (EMG) signals can be recorded by the biological electrodes (Fig. 5e and f). Temperature fluctuations in biological tissues are closely linked to pathological symptoms such as inflammation. Gold-based temperature sensors characterize the temperature variation of the environment through changes in resistance (Fig. 5g and Fig. S21). Furthermore, the coaxial dot-ring gold electrodes that make up the hydration sensors can record the variation in organ hydration by measuring electrical impedance. Fig. 5h shows the decay in skin hydration following the application of moisturizing lotion over serval minutes. Additionally, the microfabricated heater can also be used for heating therapy or to assist in controlling drug release, with its temperature adjustable by modulating the current (Fig. 5i). These electronic functionalities integrated onto MHRs serve as just a glimpse into the vast potential of this platform. The scalability of microfabrication and the proposed assembly methods open avenues for the integration of numerous other metal and semiconductor materials to provide diverse functionalities.

Discussion

In conclusion, we have developed a programmable MHR capable of loading and manipulating a diverse range of medications. Besides, the integration of miniaturized microfabricated electronics endows the MHRs with physiological sensing capabilities while maintaining their ability to proceed mechanical deformation. Due to the broad applicability and scalability of our preparation method, more advanced multifunctional bioelectronics can be integrated into the robotic system, such as high-density electrodes, electrical stimulation modules, and electrochemical sensors. Furthermore, the integration of wireless modules and power supply units can enable fully implantable systems to achieve bidirectional communication between external control hardware and electronic active prosthetics, thereby completing the closed loop of diagnosis and therapy. This advancement can significantly expand the toolbox for implantable electronics and robotic systems. Additionally, research on self-powered solutions and biodegradable materials can bring implantable magnetically controlled robots closer to practical applications.

Methods

Materials

Aramid nanofibers (ANFs; Kevlar Type 979; DuPont) and Poly (vinyl alcohol) (PVA; Mw: 146,000–186,000; Sigma-Aldrich 363065) were applied to fabricate magnetic ANF-PVA hydrogel. Potassium hydroxide (KOH; Sigma-Aldrich 484016) provided an alkaline environment for dissolving ANFs. Cellulose (cotton linter pulp) with an α-cellulose content of $>$ 95 % was purchased from Alibaba. Urea (Aladdin; U141075) and lithium hydroxide monohydrate ($LiOH{\cdot}H_2O$; Aladdin; L104907) are components of aqueous solutions for dissolving cellulose. Epichlorohydrin (EPI; Aladdin; E108184) was used as a crosslinker for the cellulose hydrogel. Poly (ethylene glycol) diacrylate (PEGDA; Mw: 700; Sigma-Aldrich 455008) is the monomer used for the second crosslinking networks in the hydrogels, while photoinitiator is 2-Hydroxy-4′-(2-hydroxyethoxy)-2-methylpropiophenone (Irgacure 2959; Sigma-Aldrich 410896). NdFeB microparticles with an average size of 5 μm (MQFP-B-F00383; Magnequench) were added into hydrogel as a magnetic component. Tetraethyl orthosilicate (TEOS, Sigma-Aldrich) and ammonium hydroxide (A.H., 29 wt% Sigma-Aldrich) were applied to generate silica dioxide (SiO_2) around the magnetic particles. Polydimethylsiloxane (PDMS; Sylgard 184; Dow Corning) is an elastomer that is treated with Benzophenone (Aladdin, B103861) for the construction of MHRs. Rhodamine (Sigma-Aldrich) and Oil Red O (Aladdin) was used to imitate the drug delivery. Dimethyl sulfoxide (DMSO), PEG-200, and glycerol were purchased from Sigma-Aldrich. 1H, 1H, 2H, 2H-perfluorodecyltriethoxysilane were purchased from Tokyo Chemical Industry Corporation. Silica nanoparticles (15 nm) were purchased from Shanghai Maikun Chemical Co., Ltd., China.

For the microfabrication, poly (methyl methacrylate) (PMMA; M.W. 350 k; Sigma–Aldrich 445746) was used as a sacrificial layer. Water-soluble tape (3 M) can assist in the transfer printing process. Polyimide (P.I.; Sigma–Aldrich 575801) was used as encapsulation material. Photoresist (AZ 5214) and wet etching were employed to define functional layer patterns and achieve selective encapsulation.

Synthesis of magnetized hydrogels

Silica nucleated around magnetic particles through hydrolysis and polycondensation of TEOS. 20 g NdFeB particles were added into 500 ml of ethanol with uniform mixing. Subsequently, 30 ml of 29 % A.H. and 1 ml of TEOS were added dropwise to the mixture. After stirring for 12 h and washing with acetone multiple times, silica-coated magnetic particles can be obtained [28].

2 wt% ANF pulp was dissolved in DMSO solvent according to the reported method [29] and then mixed with coated NdFeB particles. 10 wt% PVA DMSO solution was added into the ANF precursor with an ANF-to-PVA ratio of 1:5. The mixture was vigorously stirred to ensure thorough mixing under an inert environment. The blade-coated method and mold-assisted technology were applied to manufacture hydrogels with desired shapes. After immersing the precursor in deionized water for 24 h, ANF-PVA magnetic hydrogel can be generated. Finally, an impulse magnetizer (IM-10–30, ASC Scientific) was used to magnetize the hydrogel to obtain ANF-PVA magnetized hydrogel. Unless otherwise stated, the experiments in this paper used this hydrogel.

Cellulose precursor solution (6 wt%) was prepared by dissolving cotton linter pulp in a precooled 4.5 wt% LiOH/15 wt% urea/4 wt% EPI aqueous solution. After vigorously mechanical stirring and removing air bubbles, a cellulose precursor can be obtained. Coated NdFeB microparticles were added into cellulose precursors with homogeneous mixing. The resultant solution was transferred into customized molds or coated as a film and kept at 5℃ for 8 h to generate crosslinking networks. After washing with deionized water, cellulose magnetic hydrogels were prepared. Finally, an impulse magnetizer was used to magnetize the hydrogel to obtain magnetized cellulose hydrogel.

Preparation of MHRs

The patterned PDMS membrane was immersed in benzophenone solution (10 wt% in acetone) for more than 10 mins. Then, the PDMS was washed three times with ethanol and dried with nitrogen gas. The magnetized hydrogels with designed geometries were soaked in PEGDA

aqueous solutions composed of 20 wt% PEGDA monomer and 2 wt% initiator for 24 h. Next, the soaked magnetized hydrogels were picked out and then carefully assembled with freshly treated PDMS at the designed positions followed by UV irradiation for an hour, during which the PEGDA covalently crosslinked with benzophenone on the elastomer surface.

Preparation of MHRs with multifunctional sensing

Multifunctional microfabricated electronics were prepared using our previous method [30,31]. Briefly, a combination of vacuum deposition, photolithography, and etching techniques were employed to fabricate multilayer electronics on a 4-inch silicon wafer. Water-soluble tapes were regarded as stamps to pick up multifunctional electronics from silicon wafers. PDMS films with designed shapes were then obtained either through the model casting method or mechanical cutting. Next, a bilayer of titanium (Ti) and silicon dioxide (SiO_2) was sputtered (Denton Desktop Pro) on the tape-supported electronics. Microfabricated electronics were bonded on the PDMS film when both were treated with plasma. Finally, the PDMS-bonded electronics were prepared by releasing the tape in water. The elastomers with multifunctional sensing can also be treated with benzophenone and then bonded with magnetized hydrogel according to the method outlined above. The following assembly procedures have no impact on the electronic performance because these devices consist of inorganic electronic materials.

Preparation of Janus MHRs

After finishing the preparation of MHRs according to the above method, a superhydrophobic surface can be fabricated on the elastomer surface of MHRs [32]. A suspension of polysiloxane-coated silica was prepared as follows. Firstly, silica nanoparticles (0.1 g) were dispersed in a solution including 44 ml of ethanol and 6 ml of A.H. After mixing well, 150 μl of 1H,1H,2H,2H-perfluorodecyltriethoxysilane and 150 μl of TEOS were added with vigorous stirring. The suspension of polysiloxane-coated silica was obtained through hydrolytic condensation. This suspension can be spray-printed onto glass surfaces or PDMS surfaces to form a superhydrophobic coating. The measurements of contact angles were conducted using a contact angle measuring system (DataPhysics, OCA 25).

Structural characterization of magnetic hydrogel

SEM characterization (Hitachi S4800 FEG) was applied to demonstrate the structure of magnetic hydrogel (Fig. S13). The hydrogel samples were immersed in ethanol for 12 h followed by critical point drying (CPD; Tousimis Autosamdri 931) to generate SEM samples. TEM (FEI Tecnai G2 20 scanning TEM) is employed to characterize the silica coating layer of magnetic microparticles. The coated microparticles are dispersed in ethanol, and then the ethanol is dropped onto a copper grip for TEM examination.

Magnetic characterizations

The magnetic moment density (magnetization) of hydrogel samples was applied to evaluate the quality of alignment of the magnetic particles. The magnetic moment of the samples was measured against a sweep of external magnetic fields from −2 T to 2 T produced by a vibrating sample magnetometer (VSM, LakeShore e8600). Remanent magnetization (Fig. S5) can be calculated by dividing the magnetic moment by the volume of each sample. The magnetic particle content was calculated by:

$$C_{\mathrm{mp}} = \frac{W_{\mathrm{mp}}}{W_{\mathrm{mp}} + W_{\mathrm{precursor}}} \times 100\%$$

C_{mp} is the weight fraction of magnetic particles, W_{mp} is the weight of the magnetic particles, and $W_{\mathrm{precursor}}$ is the weight of the magnetic hydrogel precursor solution. Unless otherwise stated, all experiments demonstrated in this paper were conducted using magnetic hydrogels with a magnetic particle content of 10 %.

Mechanical testing

A tensile tester (Zwick Roell) was used to characterize the tensile responses of magnetic hydrogels and the interfacial toughness of hydrogel-elastomer hybrids. The peeling force at the steady state can be recorded by the tester. The interfacial toughness was calculated by dividing the measured peeling force by the width of the hydrogel sample.

Analytical model and FEA simulation

The magnetized hydrogel integrated on both sides of the elastomer film can drive the hinge section to bend. We can assume that the magnetized hydrogels will not bend since the modulus of hydrogel is relatively high. Therefore, the magnetized hydrogel can be viewed as a pair of magnetic dipoles in the magnetic field. The magnetic dipole moment can be expressed as:

$$\boldsymbol{\mu} = \mathbf{M} \times V \tag{1}$$

where $\boldsymbol{\mu}$ is the magnetic dipole moment, $\mathbf{M}$ is the remnant magnetization of the magnetized hydrogel, and V is the volume of the magnetized hydrogel. The ANF-PVA magnetized hydrogel containing 20 wt% NdFeB particles ($M = 27.2\ \mathrm{kA\ m^{-1}}$) were used as in Fig. 2g analysis. The volume of the magnetized hydrogel is 80 $\mathrm{mm^3}$ ($L_{\mathrm{h}} = 10$ mm, $T_{\mathrm{h}} = 1$ mm, $W_{\mathrm{h}} = 8$ mm). The magnetic dipole will produce a bending moment in a uniform magnetic field, which is the driving moment of the simply supported beam. The bending moment can be expressed as:

$$\boldsymbol{\tau} = \boldsymbol{\mu} \times \mathbf{B} \tag{2}$$

where $\boldsymbol{\tau}$ is the bending moment, $\mathbf{B}$ is the magnetic flux density of the externally applied magnetic field. As shown in Fig. S10b, a pair of moments with opposite directions and equal magnitudes are exerted on the hinge structure of the elastomer sheet. Performing a mechanical analysis on the simply supported beam model, we can obtain:

$$\boldsymbol{\tau} + \mathbf{F}y = 0 \tag{3}$$

$$\frac{\tau}{EI} = \frac{d^2y}{d^2x} \tag{4}$$

Where $\mathbf{F}$ is the internal force of the beam, y is the deflection of the beam, E is the Young modulus of elastomer (1.17 MPa), I is the moment of inertia ($I = \frac{W_{\mathrm{e}}T_{\mathrm{e}}^3}{12}$), Combining formulas (3) and (4), the maximum of deflection y can be obtained while $x = \frac{L_{\mathrm{e}}-L_{\mathrm{h}}}{2}$:

$$y_{\max} = \frac{\tau}{F} = \frac{12\mu B(L_{\mathrm{e}} - L_{\mathrm{h}})^2}{\pi^2 E W_{\mathrm{e}} T_{\mathrm{e}}^3} \tag{5}$$

As shown in Fig. 2g, the deflection y is a function of the thickness of the elastomer when other dimensions of the elastomer remain unchanged ($L_{\mathrm{e}} = 5$ mm, $W_{\mathrm{e}} = 8$ mm).

For FEA simulation, commercial software (ABAQUS) was used to calculate the energy release rate of the hydrogel-elastomer hybrid. Both the elastomer and magnetic hydrogel were assumed to be elastic materials, which were modeled as the Neo-Hookean model. The Poisson's ratio (ν) and Young's modulus (E) are as follows: $\nu_{\mathrm{elastomer}} = \nu_{\mathrm{hydrogel}} = 0.49$, $E_{\mathrm{elastomer}} = 1.17\ MPa$, $E_{\mathrm{hydrogel}} = 0.156\ MPa$. To simulate the initial crack, a seam was assigned at the edge of the hydrogel and elastomer interface. The energy release rate around the crack tip can be computed by J-integral when the meshes around the crack tip are

controlled to circular contours.

Cell culture

The mouse embryonic fibroblast NIH 3T3 cells were applied to examine the biocompatibility of magnetic hydrogels. After washing the samples with ethanol and phosphate buffered saline (PBS, Gibco pH 7.4 basic (1 ×)), the samples were immersed in fresh medium consisting of 89 vol% Dulbecco's modified Eagle medium (DMEM, Gibco, high glucose), 10 vol% fetal bovine serum (Gibco, qualified, Brazil), and 1 vol % penicillin–streptomycin (Gibco, 10,000 U mL^{-1}) for 48 h to absorb any released chemical compounds. The cell suspension was added into culture plates, followed by addition of the medium containing the released compounds. The plates were placed into an incubator at 37 ℃ and 5 % CO_2 and then the cell viability was quantified by the live/dead assays on day 1,3, and 5. The cells were observed using a fluorescent microscope (Nikon Eclipse Ci-L, Japan).

Physiological recordings

The multifunctional electronics bonded on the MHR include four biological electrodes, two pairs of bipolar electrodes, two temperature sensors, two hydration sensors, and two heaters. Electrophysiological signals were measured by a commercial data acquisition system (PowerLab T26, A.D. Instruments). Skin impedance, hydration, and temperature were recorded with an LCR meter (E4980AL; Keysight Instruments). All human experiments were performed upon approval from the Human Research Ethics Committee, The University of Hong Kong, under project number EA1812001. In addition, written consent was acquired from the participants of the research.

Author contributions

H.L., L.X. and L.W. conceived the research. H.L. carried out the experiments. L.X. and L.W. supervised the project. Other authors contributed to the experiments and analyses. H.L., L.X., and L.W. co-wrote the manuscript.

CRediT authorship contribution statement

Hegeng Li: Writing – review & editing, Writing – original draft, Visualization, Project administration, Methodology, Investigation, Data curation, Conceptualization. **Shaojun Jiang:** Visualization, Methodology, Data curation. **Qiyu Deng:** Visualization, Resources, Methodology, Data curation. **Wei Li:** Methodology, Investigation. **Weixin Zhang:** Software, Methodology. **Hengjia Zhu:** Methodology. **Zhipeng Zhao:** Methodology. **Yiyuan Zhang:** Writing – review & editing. **Liqiu Wang:** Writing – review & editing, Writing – original draft, Supervision, Funding acquisition, Conceptualization. **Lizhi Xu:** Writing – review & editing, Writing – original draft, Supervision, Resources, Investigation, Funding acquisition.

Declaration of competing interest

The authors declare that they have no known competing financial interests or personal relationships that could have appeared to influence the work reported in this paper.

Acknowledgments

We thank Dr. Yiyuan Zhang and Dr. Jiaoyuan Lian for the discussion and comments. We also thank Dr. Yong Hou for the help on cell culture. L.X. acknowledges funding support from Research Grants Council (RGC) (Project 17200320, 17200722, 17201523, 17209524 and C6004-22Y) and Environment and Conservation Fund (project 125/2021). This study was also supported by the InnoHK initiative of the Innovation and Technology Commission of the Hong Kong Special Administrative Region Government. L.W. acknowledges funding support from Research Grants Council (RGC) (Project GRF 17213823, 17205421, and 17204420) and The Hong Kong Polytechnic University (SHS Chair Professor: P0045687).

Appendix A. Supplementary data

Supplementary data to this article can be found online at https://doi.org/10.1016/j.mattod.2025.05.008.

Data availability

The authors declare that the data supporting the findings of this study are provided in the article and its supplementary materials.

References

[1] Y. Kim, X. Zhao, Magnetic soft materials and robots, Chem. Rev. 122 (2022) 5317–5364.
[2] Q. Ze, et al., Soft robotic origami crawler, Sci. Adv. 8 (2022) eabm7834.
[3] L. Wang, et al., Evolutionary design of magnetic soft continuum robots, Proc. Natl. Acad. Sci. U.S.A. 118 (2021) e2021922118.
[4] Y. Yan, et al., Soft magnetic skin for super-resolution tactile sensing with force self-decoupling, Sci. Robot. 6 (2021) eabc8801.
[5] J. Cui, et al., Nanomagnetic encoding of shape-morphing micromachines, Nature 575 (2019) 164–168.
[6] Q. Wang, et al., Magnetoactive liquid-solid phase transitional matter, Matter 6 (2023) 855–872.
[7] T. Xu, et al., Millimeter-scale flexible robots with programmable three-dimensional magnetization and motions, Sci. Robot. 4 (2019) eaav4494.
[8] S. Jiang, et al., Magnetic Janus origami robot for cross-scale droplet omni-manipulation, Nat. Commun. 14 (2023) 5455.
[9] X. Yang, et al., An agglutinate magnetic spray transforms inanimate objects into millirobots for biomedical applications, Sci. Robot. 5 (2020) eabc8191.
[10] X. Liu, et al., Magnetic living hydrogels for intestinal localization, retention, and diagnosis, Adv. Funct. Mater. 31 (2021) 2010918.
[11] M. Hua, et al., Strong tough hydrogels via the synergy of freeze-casting and salting out, Nature 590 (2021) 594–599.
[12] L. Xu, et al., Water-rich biomimetic composites with abiotic self-organizing nanofiber network, Adv. Mater. 30 (2018) 1703343.
[13] N. Xia, et al., Decoupling and reprogramming the wiggling motion of midge larvae using a soft robotic platform, Adv. Mater. 34 (2022) 2109126.
[14] N. Du, et al., Stimuli-responsive hydrogel actuators for skin therapeutics and beyond, Soft Sci. 4 (2024) 35.
[15] Z. Ren, et al., Multi-functional soft-bodied jellyfish-like swimming, Nat. Commun. 10 (2019) 2703.
[16] X. Gong, et al., Athermal shape memory effect in magnetoactive elastomers, ACS Appl. Mater. Interfaces 12 (2020) 16930–16936.
[17] W. Hu, et al., Small-scale soft-bodied robot with multimodal locomotion, Nature 554 (2018) 81–85.
[18] Y. Kim, et al., Printing ferromagnetic domains for untethered fast-transforming soft materials, Nature 558 (2018) 274–279.
[19] Y. Hui, et al., Three-dimensional printing of soft hydrogel electronics, Nat. Electron. 5 (2022) 893–903.
[20] N.M. Larson, et al., Rotational multimaterial printing of filaments with subvoxel control, Nature 613 (2023) 682–688.
[21] X. Kuang, et al., Magnetic dynamic polymers for modular assembling and reconfigurable morphing architectures, Adv. Mater. 33 (2021) 2102113.
[22] J. Zhang, et al., Voxelated three-dimensional miniature magnetic soft machines via multimaterial heterogeneous assembly, Sci. Robot. 6 (2021) eabf0112.
[23] Y. Dong, et al., Untethered small-scale magnetic soft robot with programmable magnetization and integrated multifunctional modules, Sci. Adv. 8 (2022) eabn8932.
[24] C. Wang, et al., & Sitti, M. In situ sensing physiological properties of biological tissues using wireless miniature soft robots, Sci. Adv. 9 (2023) eadg3988.
[25] E. Song, et al., Materials for flexible bioelectronic systems as chronic neural interfaces, Nat. Mater. 19 (2020) 590–603.
[26] A. Zhang, et al., Ultraflexible endovascular probes for brain recording through micrometer-scale vasculature, Science 381 (2023) 306–312.
[27] S.R. Madhvapathy, et al., Implantable bioelectronic systems for early detection of kidney transplant rejection, Science 381 (2023) 1105–1112.
[28] Y. Kim, et al., Ferromagnetic soft continuum robots, Sci. Robot. 4 (2019) eaax7329.
[29] J. Lyu, et al., High strength conductive composites with plasmonic nanoparticles aligned on aramid nanofibers, Adv. Funct. Mater. 26 (2016) 8435–8445.

[30] H. Li, et al., Breathable and skin-conformal electronics with hybrid integration of microfabricated multifunctional sensors and kirigami-structured nanofibrous substrates, Adv. Funct. Mater. 32 (2022) 2202792.
[31] H. Liu, et al., Robust and multifunctional kirigami electronics with a tough and permeable aramid nanofiber framework, Adv. Mater. 34 (2022) 2207350.
[32] W. Li, et al., Liquid repellency enabled antipathogen coatings, Mater. Today Bio 12 (2021) 100145.